33rd Annual International Conference of the IEEE EMBS
Boston, Massachusetts USA, August 30 - September 3, 2011

SUBCELLULAR PARTICLES TRACKING IN TIME-LAPSE CONFOCAL MICROSCOPY IMAGES

Shuo Li, Kate Luby-Phelps, Baoju Zhang, Xiaorong Wu, and Jean Gao

Abstract— **Automatically tracking and analyzing the mobility of live subcellular structures will expedite the understanding of signaling pathways, protein-protein interaction, drug delivery, protein synthesis and functionality. Traditional computer vision tracking methods produce yet-to-be-satisfactory results due to the complexity of the particles recorded in spatial-temporal video sequences from confocal images. The difficulties arise from diverse modalities of motion patterns (translational, Brownian, or sessile), changes in behavior during tracking, and cluttered background. In this paper, we present an effective framework to detect and track subcullular particles in different motion modalities. The methodology begins with a Divergence Filter design for motion modality detection. After that, an improved á trous wavelet is presented for segmenting particles. Represented by Euclidean Distance Map which contains information on object position, size, and intensity, the multiple particle tracking is carried out by solving a linear assignment problem. The proposed framework can also simultaneously evaluate particle population change by automatically counting the number of newly appeared or disappeared particles in time space.**

Index Terms— **Divergence Filter, subcellular structure, particle detecting, tracking, confocal microscopy**

I. INTRODUCTION

Understanding the mobility of subcellular particles like organelles, vesicles, or mRNAs is critical to understand how cells regulate delivery of specific proteins from the site of synthesis to the site of action at subcellular level. The knowledge of regulation and how it is deranged in various diseased or malfunctioned states will eventually lead to a better understanding of such diseases as diabetes, hypercholesterolemia, and many viral infections.

In order to fully understand the details of these essential processes, it is necessary to track the behavior of individual particles and to gather statistics about their mobility. Fortunately, many types of particles can be visualized specifically by tagging them with fluorescent marker proteins [1]. Modern microscopes permit the acquisition of high-speed time-lapse movies showing the behavior of the entire population of tagged particles simultaneously [2]. At least three types of particle behavior are evident in these movies: sessile vibration, Brownian, and unidirectional transport. Over time, any individual particle may switch between these three types of behavior. A first step toward understanding the stimulus and mechanism of behavior switching requires cataloging the trajectories of the entire population of particles. This cannot be done interactively, as the movies often contain over 1,000 particles per frame. The purpose of this study is to develop an algorithm for segmenting the particles and tracking them.

The complexity of subcellular dynamics poses challenges and makes the the Point Spread Function (PSF) ([3], [4]) based approaches not directly applicable here. Also, tracking multiple particles at the same time brings in fundamental difference from one single particle in terms computational complexity and approaches [5].

We define the sessile vibrates as regular motion, vice versa, the Brownian and unidirectional translation as irregular motion. In this paper, we will present a flow of algorithms for detecting and tracking subcellular particles. Our framework starts with motion modality detection by a divergence filter followed by a wavelet based particle segmentation. Features of particles of interests are selected and a score matrix is defined. In the end, the particles are tracked by solving a linear assignment and pairs linking problem.

II. METHODOLOGY

A. Particle Detection and Segmentation

To find irregular motion particles among regular ones, we developed a divergence filter [6], by which vibrating motion within a region W may be canceled out, whose property can be used as a measure of regularity and irregularity in W. The negative and positive K values, displayed in Fig. 1a, are obtained from two sequential frames, t and $t+1$. The K values actually represent the disappearing particles in frame t and appearing particles in frame $t+1$, respectively.

To detect the irregular motion particles, we need to detect those black and white spots in K-image, which needs an appropriate image segmentation technique. These spots usually have large areas but with low intensity. Thresholding methods based on pixel intensity [7] tend to miss the relatively low intensity large area spots and only keep high intensity ones even for noisy spots. Therefore an effective segmentation method should consider the size of the spots as well as individual pixel intensity.

We improved á trous wavelets as the segmentation method [8]. The convolution of K-image and the B_3-spline kernel [1/16; 1/4; 3/8; 1/4; 1/16] is computed through row by row, followed by column by column J times, where $J = \lfloor \log_2(x-1) \rfloor - 1$, and x is the minimum of image width

This work was supported by National Science Foundation under grant IIS-0546605

Shuo Li and Jean Gao are with the Computer Science and Engineering Dept., University of Texas at Arlington, Arlington, USA Emails: {shuo.li, gao}@uta.edu

Kate Luby-Phelps is with the University of Texas Southwestern Medical Center, Department of Cell Biology, Dallas, USA Email: kate.phelps@utsouthwestern.edu

Baoju Zhang and Xiaorong Wu are with College of Physics and Electronics Information, Tianjin Normal University, Tianjin, China. Emails: wdxyzbj@163.com, wu.xiaoyong@sohu.com

and image length. This operation equals to convolution with an isotropy 2D kernel. The original K-image is defined as $K_0(x, y, t)$ and the separable convolution gives a smoothed approximation $K_1(x, y, t)$, from which the wavelet plane $D_1(x, y, t)$ is defined. In general, we have,

$$D_i(x, y, t) = K_i(x, y, t) - K_{i-1}(x, y, t), \quad (1)$$

$$D_i(x, y, t) = D_i(x, y, t) / \max_{x,y}(|D_i(x, y, t)|), \quad (2)$$

with $i = 1, 2, \cdots, J$. Let:

$$Q_J(x, y, t) = \prod_{i=1}^{J} D_i(x, y, t), \quad (3)$$

Figure 1b shows the binary image result by thresholding $Q_J(x, y, t)$. The assumption is if point (x, y) is the center of a large area, its $D_i(x, y, t)$ will not easily be zero after the ith iteration, and $Q_J(x, y, t)$ will not be zero; but if point (x, y) is a small noisy area, even with high intensity, its $D_i(x, y, t)$ will easily become zero, and $Q_J(x, y, t)$ will be zero.

Here the normalization of $D_i(t)$ is added in each iteration in Eq. (2) due to the large difference among $K(t)$ values. With this normalization, a single threshold of $Q_J(x, y, t)$ for different t becomes possible.

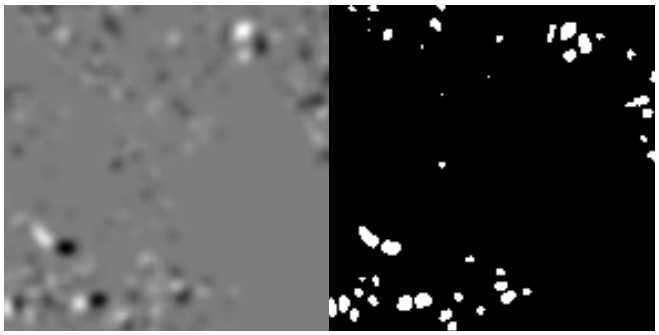

(a) Zoomed-in K image (b) segmentation result

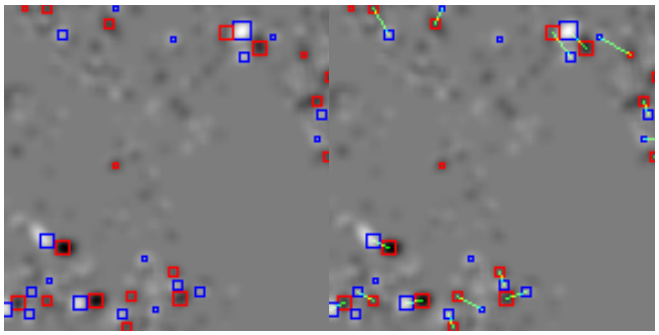

(c) representing (d) matching

Fig. 1: (a) For the purpose of visualizing K value, we set the image intensity of the point with $K(x, y, t) = 0$ as 128, so after normalization, the positive and negative K values are shown as white and black spots; (b) result of using á trous wavelets segmentation to (a); (c) The center of the square is the center of spots, and the spot size is approximated by an area of the square. (d) result of matching black and white spots in K-image.

B. Particle Feature Extraction

Assuming $I(t)$ is the tth image in the sequence, $K(t)$ is the K-image from $I(t)$ to $I(t + 1)$. Suppose there are m black spots and n white spots in $K(t)$. The Euclidian Distance Map (EDM) of $K(t)$ is $E(t) = \{E_{i,t} | i = 1, 2 \ldots m + n\}$, $E_{i,t}$ is the EDM of spot i. Vector sets $\vec{B}_t = \{\vec{B}_{i,t} | \vec{B}_{i,t} = [x_{\vec{B}_{i,t}}, y_{\vec{B}_{i,t}}, r_{i,t}]^T, i = 1, 2 \ldots m\}$ and $\vec{W}_t = \{\vec{W}_{j,t} | \vec{W}_{j,t} = [x_{\vec{W}_{j,t}}, y_{\vec{W}_{j,t}}, r_{j,t}]^T, j = 1, 2 \ldots n\}$ are used to represent each black and white spot, in which $(x_{\vec{B}_{i,t}}, y_{\vec{B}_{i,t}})$ and $(x_{\vec{W}_{j,t}}, y_{\vec{W}_{j,t}})$ are the position of the local maximum distance (LMD) value for the black and white spots, respectively, and $r_{i,t}$ or $r_{j,t}$ is the local maximum distance value of $\vec{B}_{i,t}$ or $\vec{W}_{j,t}$. The representation result is shown in Fig. 1c.

In the K-image, if one black spot $\vec{B}_{i,t}$ and one white spot $\vec{W}_{j,t}$ are close enough with similar size and image intensity, we say $\vec{B}_{i,t}$ and $\vec{W}_{j,t}$ are probably one particle moving from $(x_{\vec{B}_{i,t}}, y_{\vec{B}_{i,t}})$ in $I(t)$ to $(x_{\vec{W}_{j,t}}, y_{\vec{W}_{j,t}})$ in $I(t + 1)$. We call this matching between $\vec{B}_{i,t}$ and $\vec{W}_{j,t}$ black-white pairing. Similar to [3], this matching problem is modeled as a linear assignment problem, using a cost matrix $C(t) = \{p_{i,j,t} | i, j = 1, 2 \ldots m+n\}$ to record the costs of all possible black-white pairing and the penalty of no pairing (Fig. 2). The upper left block of $C(t)$ is defined as:

$$P(t) = \{p_{i,j,t} = \alpha_1 \bar{d}_{i,j,t} + \alpha_2 \nabla \bar{S}_{i,j,t} + \alpha_3 \nabla \bar{\kappa}_{i,j,t}\}, \quad (4)$$

where $\{i\} = \{1, 2 \ldots m\}$, $\{j\} = \{1, 2 \ldots n\}$. With

$$\bar{d}_{i,j,t} = \frac{d_{i,j,t} - \min_{i,j}(d_{i,j,t})}{\max_{i,j}(d_{i,j,t}) - \min_{i,j}(d_{i,j,t})}, \quad (5)$$

which is the normalized distance between spots i and j, with $d_{i,j,t}$ is the Euclidean distance between spot i and spot j. We define,

$$\nabla \bar{S}_{i,j,t} = \frac{\nabla S_{i,j,t} - \min_{i,j}(\nabla S_{i,j,t})}{\max_{i,j}(\nabla S_{i,j,t}) - \min_{i,j}(\nabla S_{i,j,t})}, \quad (6)$$

which is the normalized size difference between spot i and spot j with $\nabla S_{i,j,t} = |r_{i,t}^2 - r_{j,t}^2|$. We further define,

$$\nabla \bar{\kappa}_{i,j,t} = \frac{\nabla \kappa_{i,j,t} - \min_{i,j}(\nabla \kappa_{i,j,t})}{\max_{i,j}(\nabla \kappa_{i,j,t}) - \min_{i,j}(\nabla \kappa_{i,j,t})}, \quad (7)$$

which shows the normalized difference of summation of K values in black spot i and white spot j with $\nabla \kappa_{i,j,t} = \kappa_{i,t} - \kappa_{j,t}$ and $\kappa_{i,t} = \sum_{(x,y) \in i}(x, y, t)$ is the summation of K values in spot i. In Eq. (4), $\sum_{i=1}^{3} \alpha_i = 1$ and α_is are weight coefficients for each item.

For no-matching spots, the costs are $b(t)$ and $w(t)$, respectively, which are shown in the diagonal of the upper right and lower left block (Fig. 2). Thresholds are used to stop pairing two dots for the impossible situation such as far distance or large size difference, and **x** in Fig. 2 represents those situations. To make up the whole matrix $C(t)$, the lower right block is filled up with $P(t)^T$.

C. Particle Matching and Linking

With the cost matrix $C(t)$, we need to find the optimized solution path A_t:

$$min \sum_{i,j=1}^{m+n} (p_{i,j,t} A_{i,j,t}), \tag{8}$$

where $A_t = \{A_{i,j,t} | i = 1 \cdots n+m, j = 1 \cdots n+m\}$ is assignment matrix with entries 0 (no match) and 1 (match), and

$$\sum_{i=1}^{m+n} (A_{i,j,t}) = 1 \text{ and } \sum_{j=1}^{m+n} (A_{i,j,t}) = 1. \tag{9}$$

By using Hungarian Algorithm, we find the optimized solution of Eq. (8), which is the black-white pairs with the minimum global costs (Fig. 1d).

		white dots index				no pairing dots index			
		1	2	... ...	n	1	2	... ...	m
black dots index	1	$p_{1,1}$	$p_{1,2}$	... ...	$p_{1,n}$	b	x	... ...	x
	2	x	$p_{2,2}$	... ...	x	x	b	... ...	x
	⋮	⋮	⋮	... ...	⋮	⋮	⋮	... ...	⋮
	m	$p_{m,1}$	x	... ...	$p_{m,n}$	x	x	... ...	b
no pairing dots index	1	w	x	... ...	x	lower right block			
	2	x	w	... ...	x				
	⋮	⋮	⋮	... ...	⋮				
	n	x	x	... ...	w				

Fig. 2: C_t: Score matrix of black-white pairing and no pairing.

The motion trajectories of the particles are acquired by connecting the black-and-white pairing spots between K images. The decisions are made for different cases:

If $A_{i,j,t} = 1$, but no $\vec{W}_{j,t-1}$ has the same position with $\vec{B}_{i,t}$, then $\vec{B}_{i,t}$ is the start of a new track and $\vec{W}_{j,t}$ is the second point along the track;

If $A_{i,j,t-1} = 1$ and $A_{i,j,t} = 1$, and $(x_{\vec{W}_{j,t-1}}, y_{\vec{W}_{j,t-1}}) = (x_{\vec{B}_{i,t}}, y_{\vec{B}_{i,t}})$, then $(x_{\vec{B}_{i,t-1}}, y_{\vec{B}_{i,t-1}})$, $(x_{\vec{W}_{j,t-1}}, y_{\vec{W}_{j,t-1}})$, $(x_{\vec{B}_{i,t}}, y_{\vec{B}_{i,t}})$ and $(x_{\vec{W}_{j,t}}, y_{\vec{W}_{j,t}})$ belong to the same particle track;

If $A_{i,j,t-1} = 1$, but no $\vec{B}_{i,t}$ has the same position as $\vec{W}_{j,t-1}$, then $\vec{W}_{j,t-1}$ is the end of the track.

Also consider that in the end of particle representation part, we remove the redundant LMDs, which may result in that $\vec{W}_{j,t-1}$ and $\vec{B}_{i,t}$ represent the same spot, $(x_{\vec{W}_{j,t-1}}, y_{\vec{W}_{j,t-1}}) \neq (x_{\vec{B}_{i,t}}, y_{\vec{B}_{i,t}})$, but some position near $\vec{B}_{i,t}$. So we extend the range of $(x_{\vec{W}_{j,t-1}}, y_{\vec{W}_{j,t-1}})$ and $(x_{\vec{B}_{i,t}}, y_{\vec{B}_{i,t}})$ when pairing $\vec{W}_{j,t-1}$ and $\vec{B}_{i,t}$.

III. EXPERIMENTAL RESULTS

To test the effectiveness of our method, we developed experiments reflecting time-lapse sequences of cells expressing caveolin 1-GFP. The video images were taken with a Leica TCS-SP1 laser scanning confocal microscope with a 100x objective lens. The frames are of size 512×512 with a time interval of 1.2 sec, and the total number is 220. The frames can be found in `http://biolab.uta.edu:8080/tools.htm/`.

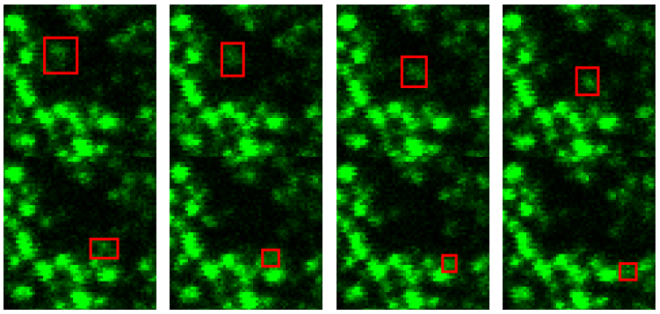

Fig. 3: Zoom-in original image cut from frame 4 to frame 11.

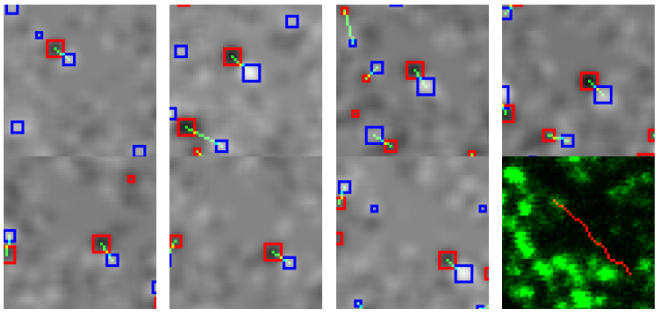

Fig. 4: Zoom-in matching results and trajectory from frame 4 to frame 11.

For better visualization, the zoomed in images of certain regions that have irregular motion particles are shown. An irregular particle with directed motion from top left to bottom right is observed from frame 4 to frame 11 (inside the red boxes in Fig. 3). Figure 4 shows the matching results of the K-image as well as a tracked particle trajectory.

Another example is given from frame 108 to frame 121. We observed the particle stops moving in three frames (114-116) during the long distance trajectory. Actually this kind of temporary suspending situation is not unusual for irregular motion particles. In order to obtain the whole trajectory of this kind irregular motion, we did the optimized matching between small trajectories considering the distance between trajectories' start points and end points as well as the directions of them. The matching results are shown in Fig. 6.

IV. DISCUSSION

Subcellular particle tracking and motion analysis are critical for cell dynamics study, which is closely related to diverse biomedical applications. In this paper, we proposed a particle tracking framework that can effectively detect, segment, and track multiple particles in directed or Brownian motion in live cell environments. The theoretical contributions of this paper come from several aspects which includes an object segmentation by developing the á trous wavelet, forming the

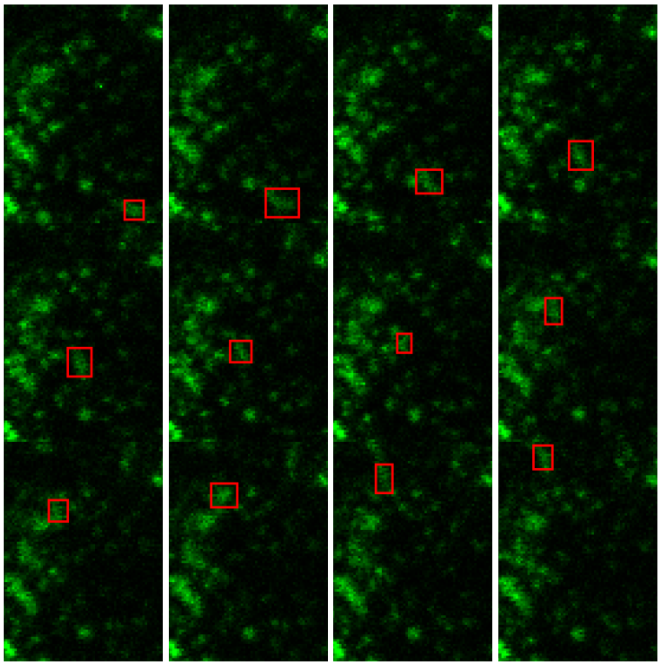

Fig. 5: Zoomed-in original image cut from frame 108 to frame 121.

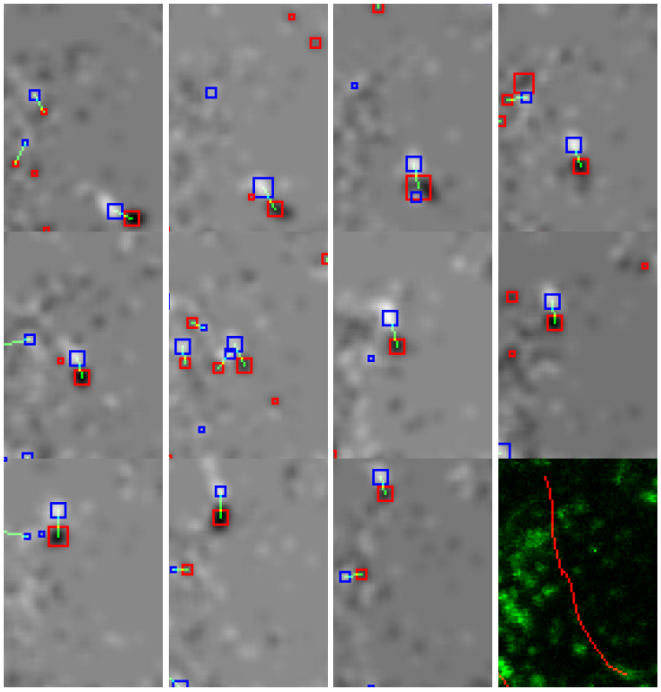

Fig. 6: Zoomed-in matching results and trajectory cut from frame 108 to frame 121.

feature score matrix for particle matching and tracking by solving a linear assignment problem.

For the future work, we intend to evaluate the matching accuracy by incorporating human-in-the-loop and the formation of a scoring matrix.

REFERENCES

[1] R. Y. Tsien, "The green fluorescent protein," *Annual Review of Biochemistry*, vol. 67, no. 1, pp. 509–544, 1998.

[2] T. Wurflinger, I. Gamper, T. Aach and A. S. Sechi, "Automated segmentation and tracking for large-scale analysis of focal adhesion dynamics," *Journal of Microscopy*, vol. 241, pp. 37–53, 2010.

[3] J. Khuloud, L. Dinah, M. Marcel, K. Hirotaka, G. Sergio, S. Sandra L, and D. Gaudenz, "Robust single-particle tracking in live-cell time-lapse sequences," *Nature Method*, vol. 5, no. 8, pp. 695–702, 2008.

[4] S. Arnauld, B. Nicolas, R. Herve, and M. Didier, "Dynamic multiple-target tracing to probe spatiotemporal cartography of cell membranes," *Nature Methods*, vol. 5, no. 8, pp. 687–694, July 2008.

[5] Q. Wen, J. Gao, A. Kosaka, H. Iwaki, K. Luby-Phelps, and D. Mundy, "A particle filter framework using optimal importance function for protein molecules tracking," *Image Processing, 2005. ICIP 2005. IEEE International Conference on*, vol. 1, pp. I–1161–4, sep. 2005.

[6] H. Iwaki, A. Kosaka, S. Li, and J. Gao, "Motion detection for subcellular structure trafficking," *Engineering in Medicine and Biology Society, 2009. EMBC 2009. Annual International Conference of the IEEE*, pp. 6722–6725, sep. 2009.

[7] M. Sezgin and B. Sankur, "Survey over image thresholding techniques and quantitative performance evaluation," *Journal of Electronic Imaging*, vol. 13, no. 1, pp. 146–168, 2004.

[8] J. Olivo-Marin, "Extraction of spots in biological images using multiscale products," *Pattern Recognition*, vol. 35, no. 9, pp. 1989 – 1996, 2002.